Polarization effect on position accuracy of fluorophore localization

Jörg Enderlein,[1] **Erdal Toprak**,[2] **Paul R. Selvin**[2,3]

[1]*Institute for Biological Information Processing 1, Forschungszentrum Jülich, D-52425 Jülich, Germany*

[2]*Center for Biophysics and Computational Biology and* [3]*Physics Dept., University of Illinois, Urbana-Champaign, U.S.A.*

Abstract: The technique of determining the position of individual fluorescent molecules with nanometer resolution, called FIONA, has become an important tool for several biophysical applications such as studying motility mechanisms of motor proteins. The position determination is usually done by fitting a 2-D Gaussian (x-y vs. photon number) to the emission intensity distribution of the fluorescent molecule. However, the intensity distribution of an emitting molecule depends not only on its position in space, but also on its three-dimensional orientation. Here, we present an extensive numerical study of the achievable accuracy of position determination as a function of molecule orientation. We compare objectives with different numerical apertures and show that an effective pixel size of 100 nm or less per CCD pixel is required to obtain good positional accuracy. Nonetheless, orientation effects can still cause position errors for large anisotropy, as high as 10 nm for high numerical aperture objectives. However, position accuracy is significantly better (< 2.5 nm) when using objectives with a numerical aperture of 1.2. Of course, probes with lower anisotropy decrease the positional uncertainty.

OCIS codes: (110.0180) Microscopy; (110.2990) Image formation theory; (260.2510) Fluorescence.

References and links

1. A. Yildiz, and P. R. Selvin, "Fluorescence imaging with one nanometer accuracy, Application to molecular motors," Acc. Chem. Res. **38**, 574-582 (2005).
2. A. Yildiz, J. N. Forkey, S. A. McKinney, T. Ha, Y. E. Goldman, and P. R. Selvin, "Myosin V walks hand-over-hand, single fluorophore imaging with 1.5-nm localization," Science **300**, 2061-2065 (2003).
3. H. Park, G. T. Hanson, S. R. Duff, and P. R. Selvin, "Nanometre localization of single ReAsH molecules," J. Microsc. **216**, 199-205 (2004).
4. G. E. Snyder, T. Sakamoto, J. A. Hammer, J. R. Sellers, and P. R. Selvin, "Nanometer localization of single green fluorescent proteins, Evidence that Myosin V walks and-over-hand via Telemark Configuration," Biophys. J. **87**, 1776-1783 (2004).
5. M. P. Gordon, T. Ha, and P. R. Selvin, "Single-molecule high-resolution imaging with photobleaching," Proc. Nat. Acad. Sci. USA **101**, 6462-6465 (2004).
6. H. Balci, T. Ha, H. L. Sweeney, and P. R. Selvin, "Interhead distance measurements in Myosin VI via SHRImP support a simplified hand-over-hand model," Biophys. J. **89**, 413-417 (2005).
7. B. Muls, H. Uji-i, S. Melnikov, A. Moussa, W. Verheijen, J. P. Soumillion, J. Josemon, K. Müllen, and J. Hofkens, "Direct measurement of the end-to-end distance of individual polyfluorene polymer chains," ChemPhysChem. **6**, 2286-2294 (2005).
8. M. J. Saxton, and K. Jacobson, "Single-particle tracking: Applications to membrane dynamics," Ann Rev Biophys Biomol Struct **26**, 373-399 (1997).
9. M. Speidel, A. Jonas, and E. L. Florin, "Three-dimensional tracking of fluorescent nanoparticles with sub-nanometer precision by use of off-focus imaging," Opt. Lett. **28**, 69-71 (2003).
10. R. E. Thompson, D. R. Larson, and W. W. Webb, "Precise nanometer localization analysis for individual fluorescent probes," Biophys. J. **82**, 2775-2783 (2002).

#70201 - $15.00 USD Received 21 April 2006; revised 3 August 2006; accepted 3 August 2006

11. M. K. Cheezum, W. F. Guilford, and W. H. Walker, "Quantitative comparison of Algorithms for tracking single fluorescent particles," Biophys. J. **81**, 2378-2388 (2001).
12. R. J. Ober, S. Ram, and E. S. Ward, "Localization accuracy in single-molecule microscopy," Biophys. J. **86**, 1185-1200 (2004).
13. A. P. Bartko, and R. M. Dickson, "Imaging three-dimensional singe molecule orientations," J. Phys. Chem. B **103**, 11237-11241 (1999).
14. M. Böhmer, and J. Enderlein, "Orientation imaging of single molecules by wide-field epi-fluorescence microscopy," J. Opt. Soc. B **20**, 554-559 (2003). In Eq. (11) of this publication, the factor *i* is erroneous and has to be replaced by –1. J.E. thanks Rolfe Petschek for finding this typo.
16. P. Török, P. D. Higdon, and T. Wilson, "Theory for confocal and conventional microscopes imaging small dielectric scatterers," J. Mod. Opt. **45**, 1681-1698 (1998).
17. J. Enderlein, "Theoretical study of detecting a dipole emitter through an objective with high numerical aperture," Opt. Lett. **25**, 634-636 (2000).
17. J. Enderlein, and M. Böhmer, "Influence of interface-dipole interactions on the efficiency of fluorescence light collection near surfaces," Opt. Lett. **28**, 941-943 (2003).
19. W. Lukosz, and R. E. Kunz, "Light emission by magnetic and electric dipoles close to a plane interface II. Radiation patterns of perpendicular oriented dipoles," J. Opt. Soc. Am. **67**, 1615-1619 (1977).
20. W. Lukosz, "Light emission by magnetic and electric dipoles close to a plane interface III. Radiation patterns of dipoles with arbitrary orientation," J. Opt. Soc. Am. **69**, 1495-1503 (1997).
20. W. Lukosz, "Light emission by multipole sources in thin layers. I. Radiation patterns of electric and magnetic dipoles," J. Opt. Soc. Am. **71**, 744-54 (1981).
21. E. H. Hellen, and D. Axelrod, "Fluorescence emission at dielectric and metal-film interfaces," J. Opt. Soc. Am. B **4**, 337-350 (1987).
22. J. D. Jackson *Classical Electrodynamics* (John Wiley, New York, 1975).
23. M. Abramowitz, and I. A. Stegun, eds., *Handbook of mathematical functions* (Harry Deutsch, Thun and Frankfurt/Main, 1984).
24. B. Richards, and E. Wolf, "Electromagnetic diffraction in optical systems II. Structure of the image field in an aplanatic system," Proc. Roy. Soc. London A **253**, 358-379 (1959).
25. J. Enderlein, T. Ruckstuhl, and S. Seeger, "Highly efficient optical detection of surface-generated fluorescence," Appl. Opt. **38**, 724-732 (1999).
26. A. M. van Oijen, J. Köhler, J. Schmidt, M. Müller, and G. J. Brakenhoff, "3-Dimensional super-resolution by spectrally selective imaging," Chem. Phys. Lett. **292**, 183-187 (1998).
27. S. W. Hell, and E. H. K. Stelzer, "Properties of a 4Pi-confocal fluorescence microscope," J. Opt. Soc. Am. A **9**, 2159-2166 (1992).
28. S. W. Hell, and J. Wichmann, "Breaking the diffraction resolution limit by stimulated emission: stimulated emission depletion microscopy," Opt. Lett. **19**, 780-782 (1994).
29. M. G. Gustafsson, D. A. Agard, and J. W. Sedat, "I/sup 5/M: 3D widefield light microscopy with better than 100 nm axial resolution," J Microsc. **195**, 10-16 (1999).

1. Introduction

The sharp image of a single fluorescing molecule is as wide as 250 nm in the visible region of the light because of the diffraction limit, which defines the resolution limit of fluorescence imaging microscopy. The lateral position of an object, however, can be localized very precisely by determining the center of its emission pattern. This is the core idea of fluorescence imaging with one nanometer accuracy (FIONA) (see Ref. [1] and citations therein). The method has found wide applications, for measuring step sizes of single motor proteins with nanometer accuracy, and for measuring small distances between fluorescent dyes or fluorescent proteins [2-7]. Even before the invention of FIONA and single molecule imaging, there exists a broad literature concerning nanometer position accuracy of fluorescing or scattering beads and its application in for the analysis of cellular structures, see e.g. [8] and references therein. One of the most advanced experimental demonstrations of the achievable sub-nanometer positional accuracy with beads is given in Ref. [9], where beads where localized with 0.8 nm precision laterally and with 4 nm axially. Thompson et al. [10] derived a theoretical expression for the accuracy with which a molecule's position can be determined, limited by several noise factors, including photon noise, fluorescent background, camera readout, and the effect of pixelation**.** They showed that the impact of all these factors can be minimized by collecting more photons. They also experimentally supported that the image center

#70201 - $15.00 USD Received 21 April 2006; revised 3 August 2006; accepted 3 August 2006

can be localized within 2 nm by using 30 nm-sized single fluorescent beads. Consequently, it was concluded that single molecules can potentially be localized with arbitrarily high precision by increasing the signal-to-noise ratio (SNR). Cheezum et al. compared different algorithms and quantitatively showed that a two-dimensional Gaussian function is the best fit to images of a single fluorescent dye if it is considered as an isotropic point source [11]. Ober et al. refined the analysis of single molecule images using a Fisher information matrix and deriving analytical estimates for the positional accuracy [12]. In all these publications, single molecules are treated as perfect isotropic emitters of light. However, as was pointed out by Bartko and Dickson [13], a single fluorescent molecule with fixed emission dipole orientation is not an isotropic emitter, and its emission strongly depends on its 3-D orientation in space.

In this paper we present a numerical analysis of FIONA experiments for molecules with fixed dipole orientation under various experimental conditions (signal strength, numerical aperture N.A. of microscope objective, pixel size of CCD) and studied the accuracy of FIONA as a function of a molecule's three-dimensional orientation. As will be seen, inclination of a molecule can introduce as much as 10 nm error in position determination when using objectives with high N.A. This error can be significantly reduced when choosing a lower N.A. objective (~ 1.2 N.A.), but at the cost of reduced light collection efficiency and not using total interference reflection excitation.

2. Theory

The electrodynamics and optics of focused and defocused imaging of single fluorescent molecules was described in Refs. [14-17]. Here, we give a brief summary of the calculations. Within the framework of classical electrodynamics, fluorescing molecules can be considered as ideal electric dipole emitters. When placed within a dielectrically homogeneous medium, such emitters exhibit the classical angular distribution of radiation proportional to $\sin^2\theta$, where θ is the angle between the direction of observation and the dipole's axis. However, when placed onto an interface separating two media with different refractive indices, that angular distribution of radiation changes dramatically due to the self-interaction of the emitting dipole with its back-reflected electromagnetic field [18-21].

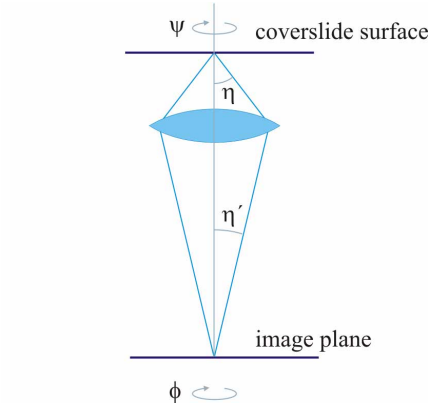

Fig. 1. Sketch of the connection between angles η and η' upon imaging. The shown lens symbolizes the whole imaging optics, i.e. both the objective and any subsequent lens such as a tube lens.

Consider a molecule embedded in water on top of a glass surface. The general geometry of imaging such a molecule is depicted in Fig. 1.

#70201 - $15.00 USD Received 21 April 2006; revised 3 August 2006; accepted 3 August 2006

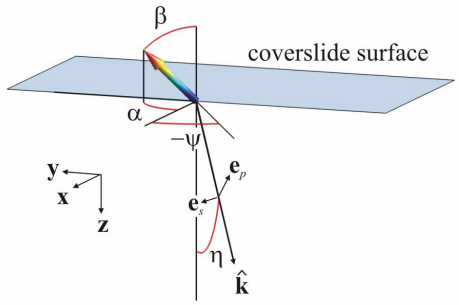

Fig. 2. Vectors and angles used in the calculation of the angular distribution of radiation and image formation.

Neglecting any constant factors, the angular distribution of the electric-field amplitude $\mathbf{E}(\eta,\psi)$generated by a dipole with orientation angles $\{\alpha,\beta\}$ along direction $\hat{\mathbf{k}}$ $\{\sin\eta\cos\psi, \sin\eta\sin\psi, \cos\eta\}$ per solid angle $\sin\eta d\eta d\psi$ is given by (see Fig. 2 and Refs. [14, 20])

$$\mathbf{E}(\eta,\psi)=\sin\beta\left[\mathbf{e}_s E_s^{\parallel}(\eta)\sin(\psi-\alpha)+\mathbf{e}_p E_p^{\parallel}(\eta)\cos(\psi-\alpha)\right]+\mathbf{e}_p\cos\beta E_p^{\perp}(\eta) \tag{1}$$

where

$$E_p^{\perp}(\eta)=\frac{nw}{w_m}\frac{q}{n_m}T_p,\ E_p^{\parallel}(\eta)=\frac{nw}{n_m}T_p,\ E_s^{\parallel}(\eta)=-\frac{nw}{w_m}T_s \tag{2}$$

α and β are the azimuthal and inclination angles of the molecule's emission dipole; $\mathbf{e}_p$ and $\mathbf{e}_s$ are orthogonal unit vectors perpendicular to the direction of radiation $\hat{\mathbf{k}}$, whereby $\mathbf{e}_s$ is also perpendicular to the optical axis (see also Fig. 2); n and n_m denote the refractive indices of glass and water, respectively; and the $T_{p,s}(\eta)$ are Fresnel's transmission coefficients [22] for plane *p*- and *s*-waves through the water/glass interface traveling along direction $\hat{\mathbf{k}}$ into the glass, and w and w_m are the *z*-components of the wave vectors in glass and water, respectively. Figure 3 visualizes the angular distribution of radiation (ADR, i.e. the angular distribution of energy radiation which is proportional to $|E(\eta,\psi)|^2$) for an inclined dipole. The angular distribution of the magnetic field amplitude is given by $\mathbf{B}(\eta,\psi) = \hat{\mathbf{k}} \times \mathbf{E}(\eta,\psi)$.

After imaging the radiation through an aplanatic optics onto the CCD camera, the electric and magnetic fields on the surface of the CCD-chip are proportional to [14-17]

$$\begin{Bmatrix} E_j \\ B_j \end{Bmatrix} = \int_0^{\eta'_{\max}} d\eta' \sin\eta' \sqrt{\frac{\cos\eta'}{\cos\eta}} \begin{Bmatrix} e_j \\ b_j \end{Bmatrix} \tag{3}$$

where we used the abbreviations

$$\begin{Bmatrix} e_x \\ e_y \end{Bmatrix} = \frac{\sin\beta}{2} \begin{Bmatrix} J_0\cos\alpha\left(\cos\eta' E_p^{\parallel} - E_s^{\parallel}\right) - J_2\cos(2\phi-\alpha)\left(\cos\eta' E_p^{\parallel} + E_s^{\parallel}\right) \\ J_0\sin\alpha\left(\cos\eta' E_p^{\parallel} - E_s^{\parallel}\right) - J_2\sin(2\phi-\alpha)\left(\cos\eta' E_p^{\parallel} + E_s^{\parallel}\right) \end{Bmatrix} \tag{4}$$
$$-i\cos\beta\cos\eta' J_1 \begin{Bmatrix} \cos\phi \\ -\sin\phi \end{Bmatrix} E_p^{\perp}$$

#70201 - $15.00 USD
Received 21 April 2006; revised 3 August 2006; accepted 3 August 2006

$$\begin{Bmatrix} b_x \\ b_y \end{Bmatrix} = \frac{\sin\beta}{2} \begin{Bmatrix} -J_0 \sin\alpha \left(E_p^{\parallel} - \cos\eta' E_s^{\parallel} \right) + J_2 \sin\left(2\phi - \alpha\right) \left(E_p^{\parallel} + \cos\eta' E_s^{\parallel} \right) \\ J_0 \cos\alpha \left(E_p^{\parallel} - \cos\eta' E_s^{\parallel} \right) - J_2 \cos\left(2\phi - \alpha\right) \left(E_p^{\parallel} + \cos\eta' E_s^{\parallel} \right) \end{Bmatrix} \qquad (5)$$
$$-i \cos\beta J_1 E_p^{\perp} \begin{Bmatrix} -\sin\phi \\ \cos\phi \end{Bmatrix}.$$

The $J_{0,1,2}$ denote Bessel functions of the first kind [23] with functional argument $k'\rho'\sin\eta'$; the k, k' are the wave vector amplitudes in glass and air, respectively. The variables ρ' and ϕ are cylindrical co-ordinates in the image plane where the field amplitudes are calculated. The angles η' and η are connected through the magnification M via Abbe's sine condition (aplanatic optics), $M \sin\eta' = n \sin\eta$, see also Fig. 1. (Here it is assumed that air has an refractive index of one). The root factor in Eq. (3) assures energy conservation during imaging [24]. Finally, the position-dependent light intensity on the CCD-chip is given by the z-component of the Poynting vector,

$$S = (c/8\pi)\mathbf{e}_z \cdot (\mathbf{E} \times \mathbf{B}^*). \qquad (6)$$

The resulting normalized intensity distribution for the ADR shown at the top of Fig. 3 is visualized at the bottom of Fig. 3.

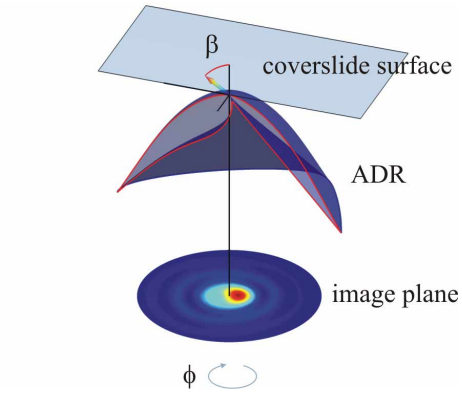

Fig. 3. Visualization of the angular distribution of radiation (ADR) and the resulting intensity distribution on the CCD for an inclined dipole emitter.

For simulating FIONA experiments, the calculated normalized intensity distribution on the CCD was multiplied with an assumed average number of detected photons, and Poissonian noise was added to each pixel using the calculated photon counts per pixel as the mean value of the Poissonian distribution. The parameters that were changed for studying the fidelity of FIONA were *effective* pixel size (CCD pixel size divided by magnification), average total number of photon counts per image (i.e. signal strength), N.A. of the imaging objective (i.e. maximum collection angle of imaging optics), and inclination angle β of the emitting molecule (i.e. angle between emission dipole and optical axis). Effective pixel size means the pixel size of the used CCD divided by the magnification of the imaging optics. Thus, even for one and the same CCD camera, effective pixel size is easily changed by changing the magnification of the optics. Of course, maximum possible magnification will be limited by the read-out noise per pixel: If too few photons are detected per pixel, read-out noise may swamp the signal.

#70201 - $15.00 USD Received 21 April 2006; revised 3 August 2006; accepted 3 August 2006

We used average photon number per image as a defining parameter, although under different experimental conditions that number will itself depends on the molecule's orientation. However, we did not like to restrict our analysis by particularities of the experimental set-up: For example, in a measurement using total internal reflection fluorescence (TIRF) excitation, molecules with vertically oriented absorption dipoles are much better excited than those with their absorption dipole parallel to the surface, in complete contrast to an experiment using conventional wide field illumination with a plane wave travelling along the optical axis. Also, as was shown in Ref. [25], relative detection efficiency of vertically and parallel oriented emission dipoles is strongly dependent on numerical aperture (N.A.) of the used objective. For example, for objectives with a N.A. larger than ca. 1.4, vertically oriented dipoles are detected with higher efficiency than in-plane dipoles.

All calculations were done for an emission wavelength of 550 nm for molecules placed in water (refractive index 1.33) on a glass surface (refractive index 1.52). This is similar to the situation encountered in measurements on motor proteins as reported in Ref. [1]. For each calculated pattern, the position of the molecule with respect to the CCD chip was chosen randomly thus averaging over different molecule positions with respect to the discrete array of CCD pixels. Having calculated a pattern on the CCD chip, a FIONA evaluation was done by fitting a two-dimensional elliptical Gaussian distribution to the pattern. The centre position (x_{fit}, y_{fit}) of the fitted Gaussian distribution was regarded as the fitted molecule position, and the difference between this position and the actual position (x_{actual}, y_{actual}) were recorded for each run of the simulation. For every set of parameters, the FIONA simulation was repeated 10^4 times with random in-plane orientation of the molecule's dipole, leading to identical distributions of position-differences $x_{fit} - x_{actual}$ and $y_{fit} - y_{actual}$.

3. Results and discussion

Figure 4 shows the images of ideal intensity distributions calculated for ten different inclination angles of a molecule's emission dipole towards the optical axis. It was assumed that imaging is done with a 1.4 N.A. objective, and the molecule is placed in water on top of a glass surface. Figure 4 also shows the circumference of fitted Gaussian distributions. Although the intensity maximum of the images can deviate by more than 100 nm from the actual position of the molecule (vertical yellow lines in the intensity images) with varying inclination angle, the center positions of the Gaussian fits show a much smaller deviation. For example, for inclination angles around 45°, the maximum of fluorescence is shifted by more than one pixel (i.e. more than 65 nm) to the left although the maximum shift of the center position of the Gaussian fits is only 16 nm. This clearly shows the advantage of a Gaussian fit instead of using a center-of-mass analysis.

#70201 - $15.00 USD Received 21 April 2006; revised 3 August 2006; accepted 3 August 2006

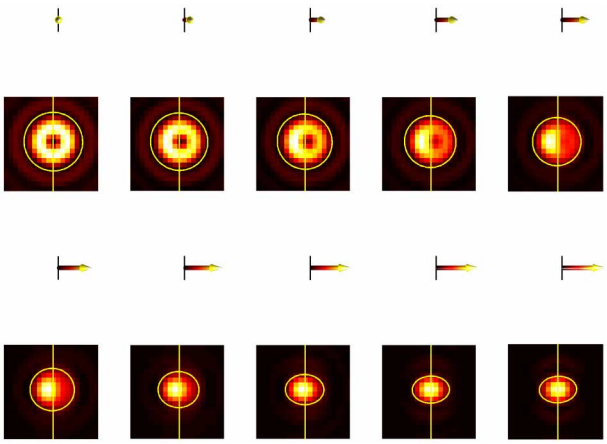

Fig. 4. Ideal intensity distributions of molecules on the CCD for different dipole inclinations towards the sample surface as indicated by the arrows depicted above each image.

The result of a FIONA simulation are the probability density distributions $P(x_{fit} - x_{actual})$ and $P(y_{fit} - y_{actual})$ of finding the difference $x_{fit} - x_{actual}$ or $y_{fit} - y_{actual}$ between fitted position $\{x_{fit}, y_{fit}\}$ and actual position $\{x_{actual}, y_{actual}\}$ along the x- and y-axis, respectively. Because the in-plane orientation of a molecule is chosen randomly for each run of the simulation, both distributions $P(x_{fit} - x_{actual})$ and $P(y_{fit} - y_{actual})$ converge to the same result. A typical result for the added distributions $P(x_{fit} - x_{actual}) + P(y_{fit} - y_{actual})$ is shown in Fig. 5 for three different dipole inclinations (0°, 45°, and 90°) of a molecule in water on a glass surface imaged with a 1.4 N.A. objective. The adopted effective CCD pixel size (i.e. pixel size divided by magnification) was 50 nm, and the average signal strength was 16000 photons per pattern. It should be remembered that the distributions show an average over all in-plane orientations of a molecule so that the two peaks seen in the distribution for 45° inclination angle corresponds to molecules pointing to the right and to the left, respectively. This is, to a more or less extent, true for all inclination angles other than 0° or 90°.

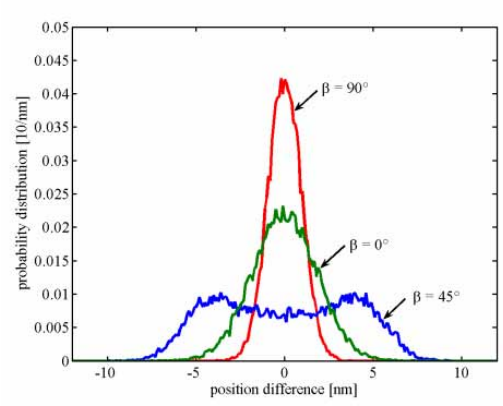

Fig. 5. Calculated probability distributions of the differences between determined and true position of a molecule for three different inclination angles as indicated. It is assumed that a molecule is placed in water on top of a glass cover slide; imaging is done with a 1.4 N.A. objective onto a CCD chip with 50 nm effective pixel size, average photon number per image was 16000.

#70201 - $15.00 USD Received 21 April 2006; revised 3 August 2006; accepted 3 August 2006

For quantifying the accuracy of FIONA by a single number we adopted the mean square deviation σ, $\sigma^2 = \langle (x_{fit} - x_{actual})^2 \rangle = \langle (y_{fit} - y_{actual})^2 \rangle$, of the position-difference distributions. For the sake of completeness it should be mentioned that the mean square deviation of the absolute position difference between fitted and actual molecule position, i.e. $\langle |\mathbf{r}_{fit} - \mathbf{r}_{actual}|^2 \rangle$, is equal to $\langle (x_{fit} - x_{actual})^2 \rangle + \langle (y_{fit} - y_{actual})^2 \rangle$ or two times σ^2. The mean square deviation can be considered as a measure of the expected error in the position determination of a molecule. We calculated position-difference probability distributions and mean-square deviations for the following experimental parameter sets, objectives with numerical apertures (N.A.) of 1.2, 1.4, 1.45 and 1.65; signal intensities (i.e. average photon counts per image) of 500, 1000, 2000, 4000, 8000, and 16000 photons; and effective CCD pixel size values of 50, 100 and 200 nm. The assumed immersion medium was water for the 1.2 N.A. objective (refractive index $n = 1.33$), oil of refractive index $n = 1.52$ for the 1.4 and 1.45 N.A. objectives, and oil with a refractive index of $n = 1.78$ for the 1.65 N.A. objective. The dependencies of the mean-square deviations (i.e. position accuracies) on dipole inclination angle are plotted in Fig. 6.

An interesting result of our analysis is the dependence of FIONA accuracy on numerical aperture. As can be seen by comparing the graphs in Fig. 6, for dipole orientations vertical or parallel to the interface ($\beta = 0°$, 90°), accuracy slightly improves with increasing N.A., but accuracy decreases for intermediate inclination angles. This is particularly prominent for high photon counts per image. The observed trend in increasing sensitivity of FIONA performance on dipole orientation with increasing N.A. can be explained when inspecting the angular distribution of radiation (ADR) shown in Fig. 3. The maximum of fluorescence emission for a dipole at an interface is emitted into the direction of total internal reflection. These emission maxima contribute most to the formation of the asymmetric and strongly orientation-dependent images on the CCD chip. Thus, by capturing more light of these emission peaks, FIONA becomes more sensitive to molecule orientation, lowering its positional accuracy. Thus, it seems that for achieving maximum position accuracy, working with a lower N.A. may be advantageous. However, a lower N.A. reduces the light collection efficiency and thus the average number of detected photons per image, which again leads to lower FIONA accuracy. In practice, one has to choose a compromise between these opposite trends.

#70201 - $15.00 USD Received 21 April 2006; revised 3 August 2006; accepted 3 August 2006

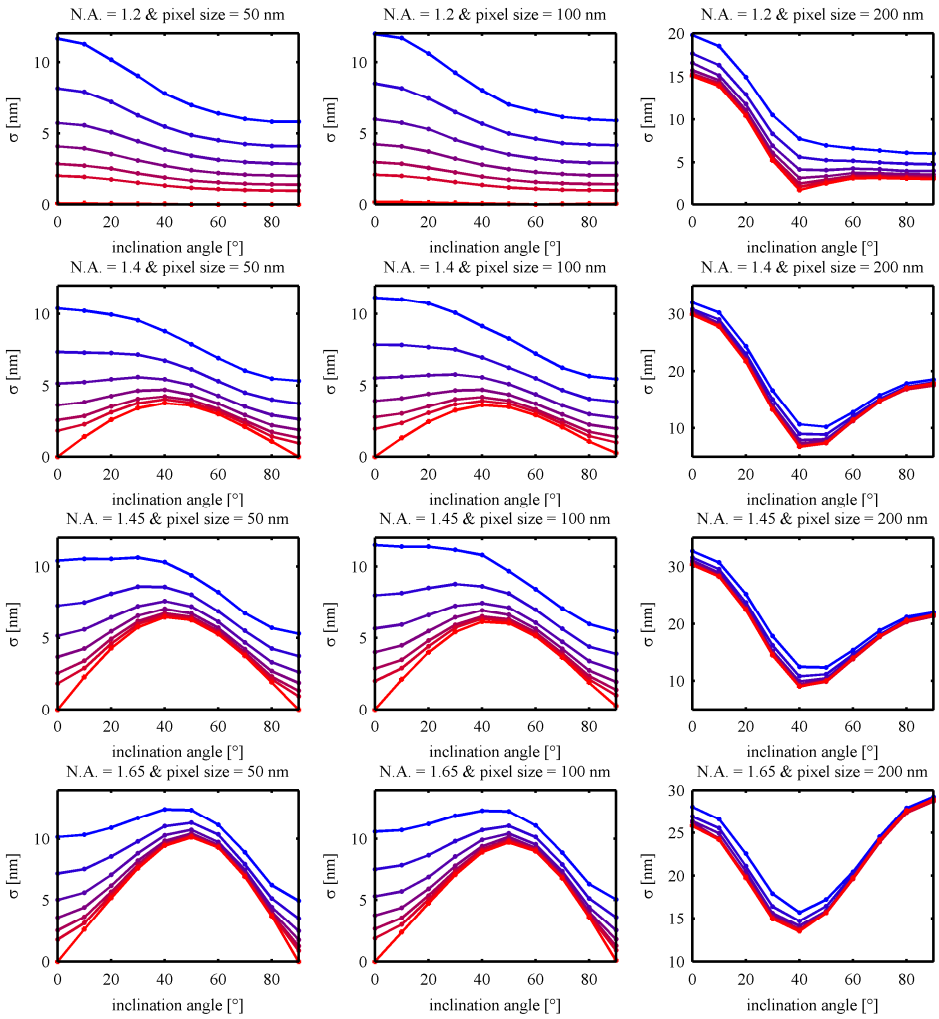

Fig. 6. Mean square deviation σ of the position difference distributions for imaging with a 1.2, 1.4, 1.45 and 1.65 N.A. objective, using a CCD camera with 50 nm, 100 nm, and 200 nm effective pixel size. Every graph shows six curves for increasing signal strength; from top to bottom 500, 1000, 2000, 4000, 8000, and 16000 and infinity number of average photons per pattern.

Another important parameter in FIONA experiments is the proper magnification, i.e. best effective pixel size (remember that effective pixel size is real CCD pixel size divided by magnification). As can be seen by comparing the graphs in Figs. 6, there is not much change in accuracy when increasing effective pixel size from 50 to 100 nm, but a sudden deterioration of FIONA performance when going to 200 nm. This 'phase transition' is easy to understand when inspecting the size of the molecule images in Fig. 4: if one has a pixel size as large as 200 nm, most of the fluorescence falls on an area of only 2 to 3 pixels wide, which makes fitting a Gaussian distribution inaccurate. Thus, for FIONA experiments, effective pixel size should not exceed 100 nm, but going to smaller pixel size only slightly improves accuracy. This can be understood when considering that although using smaller pixel size makes the molecule image larger and thus Gaussian fitting better, smaller pixel size decreases the number of photon counts per pixel making the image more noisy.

#70201 - $15.00 USD
Received 21 April 2006; revised 3 August 2006; accepted 3 August 2006

In our analysis of FIONA accuracy we assumed that the out-of-plane emission dipole orientation (inclination angle) of the imaged dye is fixed during imaging. As was seen, accuracy is lowest for intermediate inclination angles, which is easily explained when inspecting the strongly asymmetric intensity distribution for such dipoles, as shown e.g. in Fig. 4. This asymmetry makes it difficult to determine a correct center position by fitting a 2D-Gaussian distribution. If a dye is able to wobble around its attachment point (e.g. Cy3 attached DNA) during image exposure (thus emulating an isotropic emitter), the resulting image will be symmetric with respect to the actual position of the dye, and 2D-Gaussian fitting will yield better FIONA accuracy than for any of the fixed dipole orientations. The case of an isotropic emitter was considered in detail in Refs. [10-12].

In the present paper, we performed calculations for a dye emitting around 550 nm wavelength. The emission wavelength is the intrinsic length parameter in the wave-optical calculation of the molecule images on the CCD. Thus, our results hold also for different emission wavelength when the effective pixel size is appropriately rescaled. Thus, for example, the FIONA accuracy for a imaging a dye at 670 nm will be the same as for imaging a dye at 550 nm if the effective pixel in both experiments is chosen with the same ratio as the emission wavelength, i.e. 670/550. Of course, it is assumed that no additional chromatic aberration occurs with changing emission wavelength.

In our analysis, we neglected any possible background that may be present in a FIONA experiment, such as scattered light, background fluorescence, or CCD read-out noise. Our analysis presents results for the ideal case of a background-free measurement. Any additional background will only lower FIONA accuracy, but the qualitative dependence of FIONA accuracy on N.A., signal strength or pixel size will not change. A detailed analysis of the impact of background on position accuracy for isotropic emitters was already presented in Refs. [10-12], and the found general relations are also applicable to FIONA on dipoles with fixed orientation as considered here.

Our calculations regard only conventional epi-fluorescence microscopy and lateral positioning accuracy for molecules within the objective's focal plane. We did not consider position accuracy along the optical axis for molecules away from the focal plane. Also, positioning accuracy in confocal microscopy [26], or more advanced techniques such as 4Pi- [27], STED [28], or structured illumination [29] microscopy have not been considered. Studying the impact of molecule orientation on the position accuracy in these cases will be the topic of future studies.

In conclusion, we have presented detailed numerical study of FIONA on molecules with fixed dipole orientation. Our results also enable to find optimal parameters for performing FIONA on fixed dipoles. It was shown that dipole orientation cannot be neglected when estimating the accuracy of determining the position of a fluorescing molecule, and that even at highest considered signal strength (16000 photons per molecule image), one can have an position determination error as high as 10 nm when using a high-NA objective of 1.65 (see Fig. 6). This error can be minimized to 2.5 nm maximum error when going down to 1.2 NA, but at the cost of reduced flight collection efficiency. When aiming at maximum accuracy in position determination at highest light collection efficiency, one should use labels behaving as isotropic emitters such as freely rotating dyes or fluorescent beads.

Acknowledgment

We thank Dr. Sheyum Syed for many helpful discussions. This work supported by NIH AR 44420 and GM 068625 to PRS.

#70201 - $15.00 USD Received 21 April 2006; revised 3 August 2006; accepted 3 August 2006